Universal scaling of the σ field and net-protons from Langevin dynamics of model A

Shanjin Wu,[1,*] Zeming Wu,[1,†] and Huichao Song[1,2,3,‡]

[1]*Department of Physics and State Key Laboratory of Nuclear Physics and Technology, Peking University, Beijing 100871, China*

[2]*Collaborative Innovation Center of Quantum Matter, Beijing 100871, China*

[3]*Center for High Energy Physics, Peking University, Beijing 100871, China*

(Received 26 November 2018; published 5 June 2019)

In this paper, we investigate the Kibble-Zurek scaling of the σ field and net-protons within the framework of Langevin dynamics of model A. After determining the characteristic scales $\tau_{\rm KZ}$, $l_{\rm KZ}$, and $\theta_{\rm KZ}$ and properly rescaling the traditional cumulants, we construct universal functions for the σ field and approximate universal functions for net-protons in the critical regime, which are insensitive to the relaxation time and the chosen evolving trajectory. Besides, the oscillating behavior for the higher order cumulants of net-protons near the critical point is also drastically suppressed, which converge into approximate universal curves with these constructed Kibble-Zurek functions.

DOI: 10.1103/PhysRevC.99.064902

I. INTRODUCTION

The search for the critical point on the phase diagram of quantum chromodynamics (QCD) has attracted considerable attention in the heavy ion community for decades [1–6]. The critical point is the endpoint of the first order phase transition boundary that separates the quark-gluon plasma phase and the hadronic phase [1,3,7–13]. The characteristic features of the critical point are the divergence of various fluctuations, long range correlations, and singularities of some thermodynamic quantities [3]. For example, the variance σ, skewness S, and kurtosis κ of the σ field are proportional to various orders of the correlation length ξ, which diverge with ξ^2 [1,14], $\xi^{4.5}$ and ξ^7, respectively [15]. It was also found that the kurtosis κ of the σ field presents a nonmonotonic behavior with the increase of the net-baryon chemical potential μ_B [16]. After coupling the σ field with various hadrons, such critical fluctuations also influence the multiplicity distributions of conserved charges [15], which can be systematically measured in experiment.

The Beam Energy Scan (BES) program at the BNL Relativistic Heavy-Ion Collider (RHIC) aims to search the QCD critical point through evaluating the fluctuations of conserved charges [17–21]. Recently, higher order cumulants of net-protons, with the transverse momentum coverage extended to $0.4 < p_T < 2$ GeV, have been systematically measured in Au+Au collisions from 7.7 to 200 A GeV [21]. The kurtosis of net-protons in the most central collisions presents a nonmonotonic behavior and largely deviates from the poisson baseline below 39 GeV, which indicates the potential of discovering the critical point.

In the theoretical side, the equilibrium and nonequilibrium critical fluctuations near the critical point have been investigated by different groups [15,16,22–38]. Through coupling the order parameter field to the emitted protons and antiprotons on the freeze-out surface, the equilibrium critical fluctuations qualitatively explained the acceptance dependence of the measured cumulants and the nonmonotonic behavior of the kurtosis for net-protons [31,32]. However, the same framework failed to describe the cumulants C_2 and C_3 of net-protons due to the intrinsic positive contributions of the equilibrium critical fluctuations [32]. Recently, it was realized that the critical slowing down effects largely influence the non-equilibrium critical fluctuations, which even reverse the signs of skewness and kurtosis compared to the equilibrium values [29,30]. Besides, it was also found that the nonequilibrium evolution near the critical point also influences the rapidity window dependence of the variance [34]. For a qualitative and quantitative evaluation of the BES data and for the search of the critical point, it is important to develop dynamical models for the evolving bulk matter together with nonequilibrium evolution of the critical mode (for recent progresses, please also refer to the work of hydro+ [36]).

For a dynamical model near the critical point, the calculated nonequilibrium fluctuations are sensitive to various free inputs and parameters, such as the trajectory and relaxation time of the evolving system, the mapping between the three-dimensional Ising model and the hot QCD system, etc. Meanwhile, the critical slowing down effects drive the system out of equilibrium, which leads to correlated regions with characteristic length scales after the system becomes "frozen". It was realized that, within the framework of Kibble-Zurek mechanism (KZM), one could construct some universal variables near the critical point, that are independent on some of these nonuniversal factors [33,39–42]. In cosmology, the KZM was first introduced by Kibble [43] to study the defect formation of the expanding Universe after the Big Bang,

*shanjinwu2014@pku.edu.cn
†zeming_wu@pku.edu.cn
‡huichaosong@pku.edu.cn

which is then extended by Zurek [44] to study the condensed matter systems near the critical point. Recently, the KZM was applied to relativistic heavy ion collision within the framework of Fokker-Planck equation, which constructed universal functions for the evolving σ field in the critical regime [33].

In this work, we will investigate the universal scaling of both σ field and net-protons from the Langevin dynamics of model A. Compared with the Fokker-Planck equation approach which only considers the zero mode of the σ field, our Langevin dynamics simulations evolve the whole σ field in the position space event by event, which can be coupled with final hadrons to further investigate the multiplicity fluctuations and possible universal scaling of net-protons in the critical regime. Note that this paper does not aim to construct realistic universal experimental observables with this simplified Langevin dynamics, but focuses on investigating the Kibble-Zurek scaling of the σ field and net-protons with two ideal cases: 1) the systems evolve along a chosen trajectory with different relaxation times; 2) the systems evolve along different chosen trajectories. We will demonstrate that one could construct universal functions for the σ field in the critical regime, which are insensitive to the relaxation time or chosen evolution trajectory. With a linear expansion of the distribution functions of protons and antiprotons, such universal behavior of the σ field could be translated into a similar universal behavior of net-protons through the σNN coupling. On the other hand, the numerical simulations with the full distribution functions of protons and antiprotons show that one could still construct an approximate universal functions for net-protons, which drastically reduce the sensitivity to the relaxation time and evolving trajectory.

The paper is organized as follows. Section II briefly introduces Langevin dynamics of model A and the basic idea to construct the universal functions according to the Kibble-Zurek mechanism. Section III presents and discusses the constructed universal functions of the σ field and approximate universal functions of net-protons in the critical regime. Section IV summarizes and concludes the paper.

II. MODEL AND SET UPS

A. Langevin dynamics of model A

It is generally believed that the hot QCD system belongs to model H according to the classification of Ref. [45], which focuses on the dynamics of order parameter field, baryon, and energy density [24]. Recently, an alternative approach, hydro+ [36], has been developed, which extended traditional hydrodynamics to the critical regime with the additional evolution of the slow mode. However the numerical implementation of model H and hydro+ are both complicated, which are still under development.

In this paper, we focus on investigating the universal behavior of the σ field and net-protons near the critical point, with a simplified Langevin dynamics, called model A, that only evolves the nonconserved order parameter field of one single component. The corresponding equation is written as

$$\frac{\partial\sigma(\boldsymbol{x},\tau)}{\partial\tau} = -\frac{1}{m_\sigma^2\tau_{\rm eff}}\frac{\delta U[\sigma(\boldsymbol{x})]}{\delta\sigma(\boldsymbol{x})} + \zeta(\boldsymbol{x},\tau), \tag{1}$$

where the noise ζ satisfies the fluctuation-dissipation theorem:

$$\langle\zeta(\boldsymbol{x},\tau)\rangle = 0,$$
$$\langle\zeta(\boldsymbol{x},\tau)\zeta(\boldsymbol{x}',\tau')\rangle = \frac{2T}{m_\sigma^2\tau_{\rm eff}}\delta^3(\boldsymbol{x}-\boldsymbol{x}')\delta(\tau-\tau'). \tag{2}$$

Here, T is the temperature, m_σ is the mass of the σ field, $\tau_{\rm eff}$ is the relaxation time, and $U[\sigma(\boldsymbol{x})]$ is the effective potential. According to the analyses of dynamical critical behavior [45], the effective relaxation time $\tau_{\rm eff}$ depends on equilibrium correlation length $\xi_{\rm eq}$ as $\tau_{\rm eff} = \tau_{\rm rel}(\xi_{\rm eq}/\xi_{\rm min})^z$, where $\tau_{\rm rel}$ is a free parameter in this work. For the dynamical critical exponent, we use the one from model H with $z = 3$.

In the vicinity of the critical point, the effective potential $U[\sigma(\boldsymbol{x})]$ can be expanded in the powers of the order parameter field $\sigma(\boldsymbol{x})$:

$$U[\sigma(\boldsymbol{x})] = \int d^3x\Big\{\frac{1}{2}[\nabla\sigma(\boldsymbol{x})]^2 + \frac{1}{2}m_\sigma^2[\sigma(\boldsymbol{x})-\sigma_0]^2 + \frac{\lambda_3}{3}[\sigma(\boldsymbol{x})-\sigma_0]^3 + \frac{\lambda_4}{4}[\sigma(\boldsymbol{x})-\sigma_0]^4\Big\}, \tag{3}$$

where λ_3 and λ_4 are the coupling coefficients of the cubic and quadratic terms, σ_0 is the equilibrium mean value of $\sigma(\boldsymbol{x})$, m_σ is the mass of the σ field which is related to the equilibrium correlation length with $m_\sigma = 1/\xi_{\rm eq}$. Following Ref. [29], we construct the effective potential $U[\sigma(\boldsymbol{x})]$ through a mapping between the hot QCD system and the three-dimensional (3d) Ising model [46,47]. In more details, one first calculates the cumulants from the distribution function $P[\sigma] \sim \exp[-U(\sigma)/T]$ and from the parametrization of magnetization $M^{\rm eq}$ of the 3d Ising model. A comparison of the cumulants obtained from these two procedures gives the forms of $\sigma_0(R,\theta)$, $\xi(R,\theta)$, $\lambda_3(R,\theta)$, and $\lambda_4(R,\theta)$. Here, R and θ are the distance and angle with respect to the location of the critical point, which are related to the Ising model variables r and h via $r(R,\theta) = R(1-\theta^2)$, $h(R,\theta) = R^{5/3}(3\theta-2\theta^3)$. The Ising model variables $(r,\ h)$ are related to the hot QCD parameters $(T,\ \mu)$ through a linear mapping: $(T-T_c)/\Delta T = h/\Delta h$, $(\mu-\mu_c)/\Delta\mu = -r/\Delta r$. Note that such mapping is nonuniversal, which depends on the position of the critical point and the shape of the critical regime for the constructed QCD phase diagram. The details can be found in the Appendix of this paper.

To numerically solve Eq. (1), one needs to input the local temperature $T(\boldsymbol{x})$ and local chemical potential $\mu(\boldsymbol{x})$ of the external heat bath. For simplicity, we assume that the heat bath evolves along certain trajectory with uniform temperature and chemical potential in the position space. Such trajectories can be expressed with the r and h variables [33]:

$$r = r_c - a_h h^2, \tag{4}$$

where r_c and a_h are two free parameters to tune the shape of the trajectories. In the following calculations, we select two types of trajectories, called type A and type B. For type A trajectory, we set $a_h = 0$ and $r_c = 0.02\ \Delta r$. This corresponds to the system evolving with fixed chemical potential,

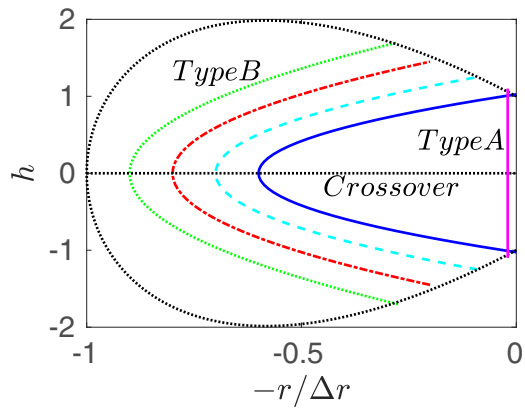

FIG. 1. Trajectories of type A (magenta line) and type B (colored curves) in the critical regime. The boundary of the critical regime (black dashed curve) is defined by $\xi_{\rm eq} = 1$ fm.

where the changing rate of the effective potential is mainly captured by the variation of the correlation length $\xi_{\rm eq}$. For type B trajectories, we set r_c as a constant, and tune a_h to ensure approximately equal correlation length near the phase transition line. In this way, θ becomes the dominated factor for the changing rate of the effective potential, which simplifies the corresponding analysis of the universal behavior for type B trajectories. In Fig. 1, we plot the trajectories of type A and type B, which are denoted by the magenta line and different colored curves, respectively. The black dashed curve is the boundary of the critical regime defined by the equilibrium correlation length $\xi_{\rm min} = 1$ fm. Note that, a more realistic trajectory of the heat bath is the line with constant baryon density over entropy n/s, which is complicate for the following computation of quench time in Sec. II B. For simplicity, we assume the system evolves along these chosen trajectories (type A and type B) in this work.

As the heat bath evolving along one of these trajectories, we assume that the temperature T drops down in a Hubble-like way [33]:

$$\frac{T(\tau)}{T_I} = \left(\frac{\tau}{\tau_I}\right)^{-0.45}, \tag{5}$$

where T_I and τ_I are the initial temperature and initial time.

In numerical simulations, we first construct the initial profiles of the σ field through the probability function: $P[\sigma(\boldsymbol{x})] \sim \exp\{-U[\sigma(\boldsymbol{x})]/T\}$ and then evolve the σ field event by event according to Eq. (1). But the discretization of the noise term leads to a grid size dependence for the calculated cumulants [48]. To avoid this complexity, we only focus on the long wavelength behavior of the evolving system and coarse-grain the noise term over the spatial extension as proposed in Ref. [49]. In other word, we numerically evolve Eq. (1) in $3+1$ dimensions and the noise term is been coarse-grained which is uniform in coordinate space but random in temporal direction. In the limit of zero mode, one can prove [50] that such Langevin equation is equivalent to the Fokker-Planck equation implemented in Ref. [29]. For each time step, we calculate the corresponding cumulants which are defined as the following:

$$\begin{aligned} C_1 &= \langle\sigma\rangle, \quad C_2 = \langle\sigma^2\rangle - \langle\sigma\rangle^2, \\ C_3 &= \langle\sigma^3\rangle - 3\langle\sigma^2\rangle\langle\sigma\rangle + 2\langle\sigma\rangle^3, \\ C_4 &= \langle\sigma^4\rangle - 4\langle\sigma^3\rangle\langle\sigma\rangle - 3\langle\sigma^2\rangle^2 + 12\langle\sigma^2\rangle\langle\sigma\rangle^2 - 6\langle\sigma\rangle^4, \end{aligned} \tag{6}$$

where σ denotes the spatial average of the sigma field $\sigma(\boldsymbol{x})$ and $\langle\cdots\rangle$ is the event average.

B. The Kibble-Zurek scaling

The above cumulants of the σ field Eq. (6) are influenced by inputs and free parameters in the model calculations, such as the relaxation time, the trajectory of the heat bath, and the mapping between the 3d Ising model and the hot QCD system, etc. Within the framework of the Kibble-Zurek mechanism, Ref. [33] has constructed some universal functions for the Fokker-Planck equation approach, which are independent on some nonuniversal factors. In this paper, we will explore such universal behavior within the framework of Langevin dynamics.

For a system evolving near the critical point, there are two competitive time scales, the relaxation time $\tau_{\rm eff}$ that describes the relaxation rate of the order parameter field and the quench time $\tau_{\rm quench}$ that describes the changing rate of the effective potential. As explained in Sec. II A, the relaxation time takes the form $\tau_{\rm eff} = \tau_{\rm rel}(\xi_{\rm eq}/\xi_{\rm min})^z$ with $z = 3$. The quench time $\tau_{\rm quench} = \min(\tau^{\xi}_{\rm quench}, \tau^{\theta}_{\rm quench})$ can be calculated as [33]

$$\tau^{\xi}_{\rm quench} = \left|\frac{\xi_{\rm eq}(\tau)}{\partial_\tau \xi_{\rm eq}(\tau)}\right|, \quad \tau^{\theta}_{\rm quench} = \left|\frac{\theta(\tau)}{\partial_\tau \theta(\tau)}\right|. \tag{7}$$

In general, the quench time decreases as the system cools down, and the relaxation time rapidly increases as the system approaches the critical point due to the critical slowing down effects. This leads to a point τ^*, where the relaxation time equals to the quench time, after which the order parameter field becomes hard to adjust itself to the changing effective potential. In other words, the system becomes approximately frozen after τ^*. Correspondingly, one defines the characteristic time scale $\tau_{\rm KZ}$, length scale $l_{\rm KZ}$, and magnetization angle $\theta_{\rm KZ}$ to characterize the typical scales of the correlated patches for the evolving systems near the critical point:

$$\begin{aligned} \tau_{\rm KZ} &= \tau_{\rm eff}(\tau^*) = \tau_{\rm quench}(\tau^*), \\ l_{\rm KZ} &= \xi_{\rm eq}(\tau^*), \quad \theta_{\rm KZ} = \theta(\tau^*). \end{aligned} \tag{8}$$

In Fig. 2, we plot the time evolution of the relaxation time $\tau_{\rm eff}$ and quench time $\tau_{\rm quench}$ along trajectories of type A (with $\tau_{\rm rel}/\tau_c = 0.02, 0.06, 0.10, 0.14$) and type B (with $r_c = 0.6, 0.7, 0.8, 0.9$). As shown in Fig. 2, the increasing relaxation time $\tau_{\rm eff}$ and decreasing quench time $\tau_{\rm quench}$ lead to a proper time τ^*, with which one could further obtain the characteristic scales $\tau_{\rm KZ}$, $l_{\rm KZ}$, and $\theta_{\rm KZ}$ from Eq. (8). Following [33], we construct the universal functions $\bar{f}_n((\tau - \tau_{\rm KZ})/\tau_{\rm KZ}, \theta_{\rm KZ})$ $(n = 1, \ldots, 4)$ through rescaling the cumulants C_n $(n = 1, \ldots, 4)$ and the proper time $\tau - \tau_c$ with these

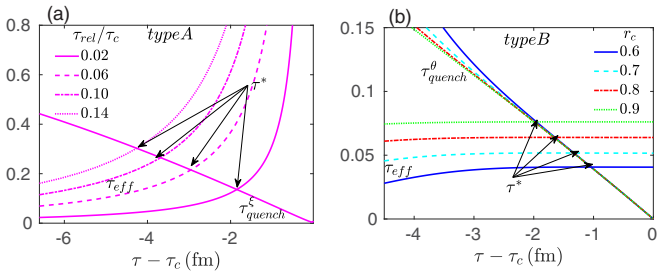

FIG. 2. Time evolution of the relaxation time $\tau_{\rm eff}$ and quench time $\tau_{\rm quench}$ along trajectory of type A with different $\tau_{\rm rel}/\tau_c$ (a) and along trajectories of type B with different r_c (b). The locations of the proper time τ^* are obtained from $\tau_{\rm eff}(\tau^*) = \tau_{\rm quench}(\tau^*)$.

characteristic scales, which is written as the following:

$$C_n(\tau - \tau_c) \sim l_{\rm KZ}^{-\frac{1}{2}+\frac{5}{2}(n-1)} \bar{f}_n[(\tau - \tau_c)/\tau_{\rm KZ}; \theta_{\rm KZ}], \quad n = 1, \ldots, 4, \tag{9}$$

where τ_c is the time when the QCD system evolves to the crossover line. The exponent of $l_{\rm KZ}$ comes from the fact that the n-order equilibrium critical cumulants are proportional to $[-1 + 5(n-1)]/2$ powers of the correlation length $\xi_{\rm eq}$ [33].

III. RESULTS AND DISCUSSIONS

In the following calculations, we first simulate the evolution of the σ field using Eq. (1), and then investigate the possible universal behavior of the σ field and net-protons. Below are detailed calculations and results.

A. Kibble-Zurek scaling of the σ field

Figure 3(a) shows the time evolution of the cumulants for the σ field, which evolves along a fixed trajectory of type A with different relaxation times, $\tau_{\rm rel}/\tau_c = 0.02, 0.06, 0.1, 0.14$. Due to the critical slowing down effects, these dynamical cumulants largely deviate from the equilibrium values, which are also sensitive to the relaxation time inputs. Figure 3(b) focuses on demonstrating the related universal behavior of the σ field. As explained in Sec. II, the changing rate of the effective potential along type A trajectory is mainly controlled by the variance of the correlation length $\xi_{\rm eq}$, and the corresponding quench time is $\tau^{\xi}_{\rm quench} = |\xi_{\rm eq}(\tau)/\partial_\tau \xi_{\rm eq}(\tau)|$. As shown in Fig. 2(a), the proper time τ^* can be obtained from comparing the relaxation time $\tau_{\rm eff}$ and the quench time $\tau^{\xi}_{\rm quench}$ with which the Kibble-Zurek scales $\tau_{\rm KZ}$ and $l_{\rm KZ}$ can be calculated from Eq. (8). With $l_{\rm KZ}$ and $\tau_{\rm KZ}$, we rescale C_n and $\tau - \tau_c$ and construct the universal functions $\bar{f}_n$ according to Eq. (9). Figure 3(b) plots the universal functions $\bar{f}_n$ for the evolving systems with different relaxation times, which converge into one universal curve near the critical point. In contrast, the original cumulants, $C_n (n = 1, \ldots, 4)$, before the rescaling procedure are separated from each other and are sensitive to the relaxation times.

In Fig. 4, we explore the universal behavior of the σ field with the heat bath evolving along different trajectories. For simplicity, we construct specific trajectories (type B) with approximately equal equilibrium correlation length $\xi_{\rm eq}$ near the crossover line, which ensures the changing rate of $\xi_{\rm eq}$ is much smaller than the one of θ. Correspondingly, the quench time can be calculated as $\tau^{\theta}_{\rm quench} = |\theta(\tau)/\partial_\tau \theta(\tau)|$. Similar to the above case, the proper time τ^* can be obtained from Fig. 2(b) and the Kibble-Zurek scales $\tau_{\rm KZ}$ and $l_{\rm KZ}$ are calculated from Eq. (8) with which the universal functions $\bar{f}_n$ can be constructed from Eq. (9). In general, $\theta_{\rm KZ}$ is a nonuniversal factor which strongly depends on the evolving trajectories. Here, we specifically tune the free parameter $\tau_{\rm rel}/\tau_c$ to ensure $\theta_{\rm KZ}$ is a constant ($\theta_{\rm KZ} = 0.1$) for these different trajectories of type B. In this case, we focus on investigating the universal scaling for such specific type of trajectories. Figure 4(a) show that various cumulants of the σ field are very sensitive to the evolving trajectory. Figure 4(b) show that, after rescaling C_n and $\tau - \tau_c$ with $l_{\rm KZ}^{[-1+5(n-1)]/2}$ and $\tau_{\rm KZ}$, the constructed

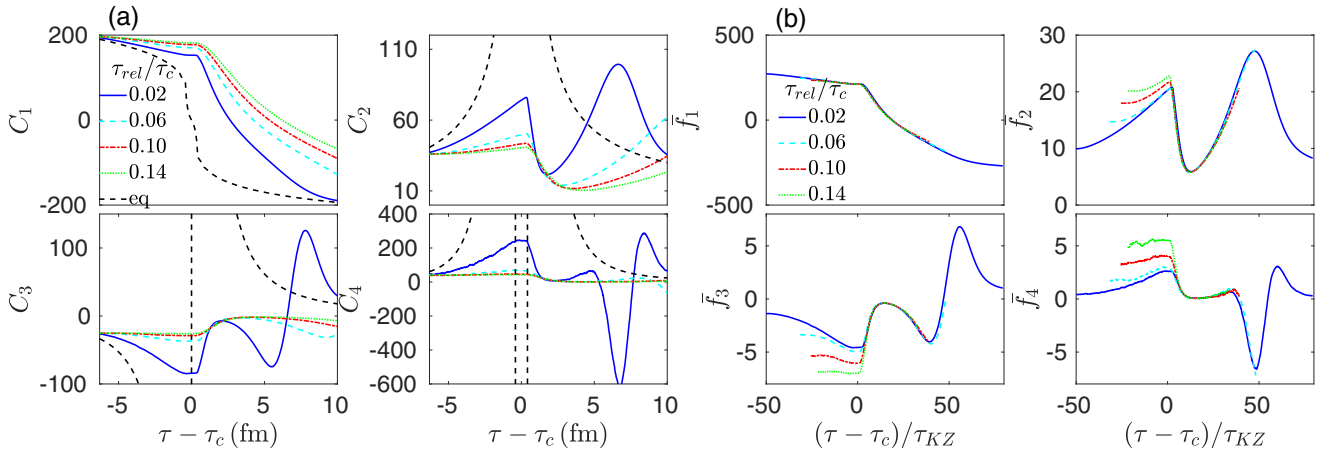

FIG. 3. (a) The cumulants $C_n (n = 1, \ldots, 4)$ of the σ field as a function of $\tau - \tau_c$, evolving along type A trajectory with $\tau_{\rm rel}/\tau_c = 0.02,\ 0.06,\ 0.1,\ 0.14$. The dashed curves represent the equilibrium cumulants along the trajectory. (b) The corresponding universal functions $\bar{f}_n((\tau - \tau_c)/\tau_{\rm KZ}, \theta_{\rm KZ})\,(n = 1, \ldots, 4)$ as a function of $(\tau - \tau_c)/\tau_{\rm KZ}$.

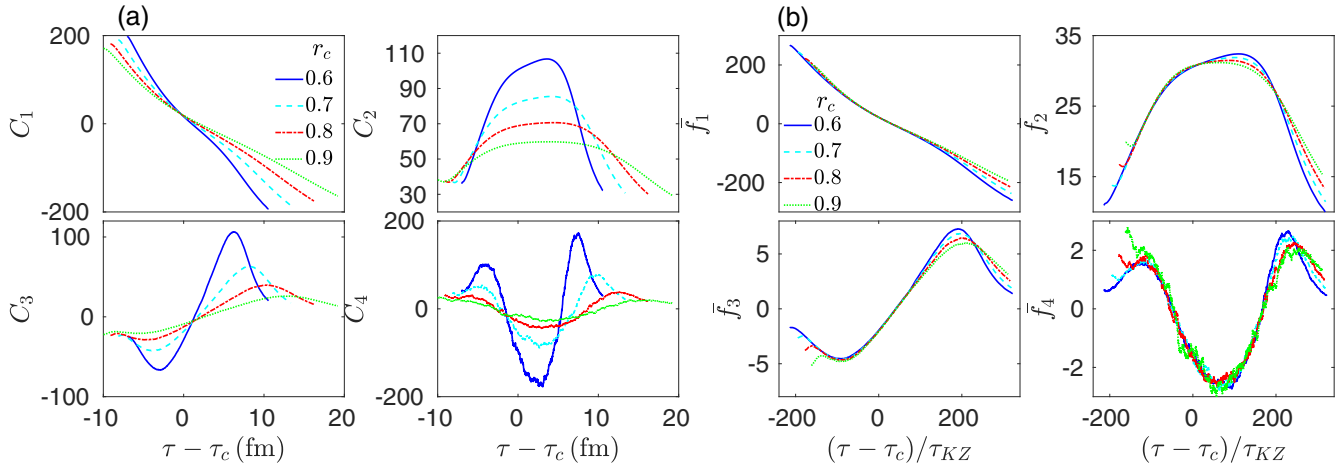

FIG. 4. Similar to Fig. 3, but evolving along type B trajectories with $r_c = 0.6,\ 0.7,\ 0.8,\ 0.9$.

universal functions $\bar{f}_n$ are independent on these chosen trajectories near the critical point.

B. Approximate Kibble-Zurek scaling of net-protons

In last subsection, we have constructed the universal functions of the σ field that evolve with different relaxation times or with different trajectories. In this subsection, we further explore the possible universal behavior of net-protons.

In Refs. [16,31,32], the multiplicity fluctuations of net-protons near the critical point are calculated with the modified distribution functions $f_{p/\bar{p}}(\boldsymbol{x}, \boldsymbol{p})$ through coupling the protons and antiprotons with the external order parameter field. For simplicity, we take the Boltzmann distribution

$$f_{p/\bar{p}}(\boldsymbol{x}, \boldsymbol{p}) = e^{-(E \pm \mu_B)/T}, \tag{10}$$

where μ_B is the baryon chemical potential, the lower/upper signs are for protons/antiprotons, and E is the energy of the particle $E = \sqrt{m^2 + \boldsymbol{p}^2}$. For these particles existed near the critical point, one generally implements a variable effective mass, $m = m_0 + \delta m$, to introduce critical fluctuations to the distribution function, where m_0 is the physical mass of the particle and $\delta m = g\sigma(\boldsymbol{x})$ comes from the interactions between the σ field and the particles with the σNN coupling [16,31,32]. In this work, we use $g = 3.3$, $m_0 = 938.27$ MeV, and set μ_B and T approximatively to critical values $\mu_c = 395$MeV, $T_c = 160$MeV as predicted in Ref. [51].

The total number of net-protons at a certain temperature T and chemical potential μ_B can be calculated through integrating $f_{p/\bar{p}}(\boldsymbol{x}, \boldsymbol{p})$ over the whole phase-space:

$$N_{p-\bar{p}} \equiv N_p - N_{\bar{p}} = d \int \frac{d^3\boldsymbol{p} d^3\boldsymbol{x}}{(2\pi)^3} [f_p(\boldsymbol{x}, \boldsymbol{p}) - f_{\bar{p}}(\boldsymbol{x}, \boldsymbol{p})], \tag{11}$$

where the degeneracy factor $d = 2$ for protons and antiprotons. With Eq. (11), we can calculate the cumulants of net-protons and investigate the possible Kibble-Zurek scaling near the critical point. First, we consider a simple case with small fluctuations of the σ field. The distribution functions $f_{p/\bar{p}}$ can be linearly expanded as [31,32]

$$f_{p/\bar{p}} = f_{p/\bar{p},0} + \delta f = f_{p/\bar{p},0}[1 - g\sigma/(\gamma T)], \tag{12}$$

where $f_{p/\bar{p},0}$ is the traditional Boltzmann distribution like the one described by Eq. (10), but replace the variable mass m by the physical mass m_0 of protons and antiprotons. δf denotes the deviation associated with the critical fluctuations from the σNN coupling and $\gamma = \sqrt{m_0^2 + \boldsymbol{p}^2}/m_0$.

With such expansion, various cumulants of net-protons can be calculated as

$$\begin{aligned}
C_{1,N} &= \left(\int_{\boldsymbol{p}} \frac{f_{p,0}(p) - f_{\bar{p},0}(p)}{\gamma(p)} \right) \langle \sigma \rangle, \\
C_{2,N} &= \left(\int_{\boldsymbol{p}} \frac{f_{p,0}(p) - f_{\bar{p},0}(p)}{\gamma(p)} \right)^2 \langle (\delta\sigma)^2 \rangle, \\
C_{3,N} &= -\left(\int_{\boldsymbol{p}} \frac{f_{p,0}(p) - f_{\bar{p},0}(p)}{\gamma(p)} \right)^3 \langle (\delta\sigma)^3 \rangle, \\
C_{4,N} &= \left(\int_{\boldsymbol{p}} \frac{f_{p,0}(p) - f_{\bar{p},0}(p)}{\gamma(p)} \right)^4 [\langle (\delta\sigma)^4 \rangle - 3\langle (\delta\sigma)^2 \rangle^2],
\end{aligned} \tag{13}$$

where the notations $\int_{\boldsymbol{p}} \equiv \frac{dg}{T} \int \frac{d^3\boldsymbol{p}}{(2\pi)^3}$ and $\delta\sigma \equiv \sigma - \langle \sigma \rangle$. These equations show that, with σNN coupling that transforms the critical fluctuations of the σ field to the critical fluctuations of protons and antiprotons, the cumulants of the net-protons are proportional to the ones of the σ field with the simplified liner expansion of Eq. (12). Correspondingly, the universal scaling of net-protons behaves as the one of the σ field as shown in Figs. 3 and 4.

For the σ field with large fluctuations, the linear expansion of Eq. (12) is no longer valid. In the following calculations, we implement the full distribution function Eq. (10) to calculate the multiplicity fluctuations of net-protons with the configurations of the σ field and then investigate the possible universal scaling behavior. Figures 5(a) and 6(a) show the time evolution of the cumulants of net-protons for a trajectory of type A with different $\tau_{\rm rel}/\tau_c$ and for trajectories

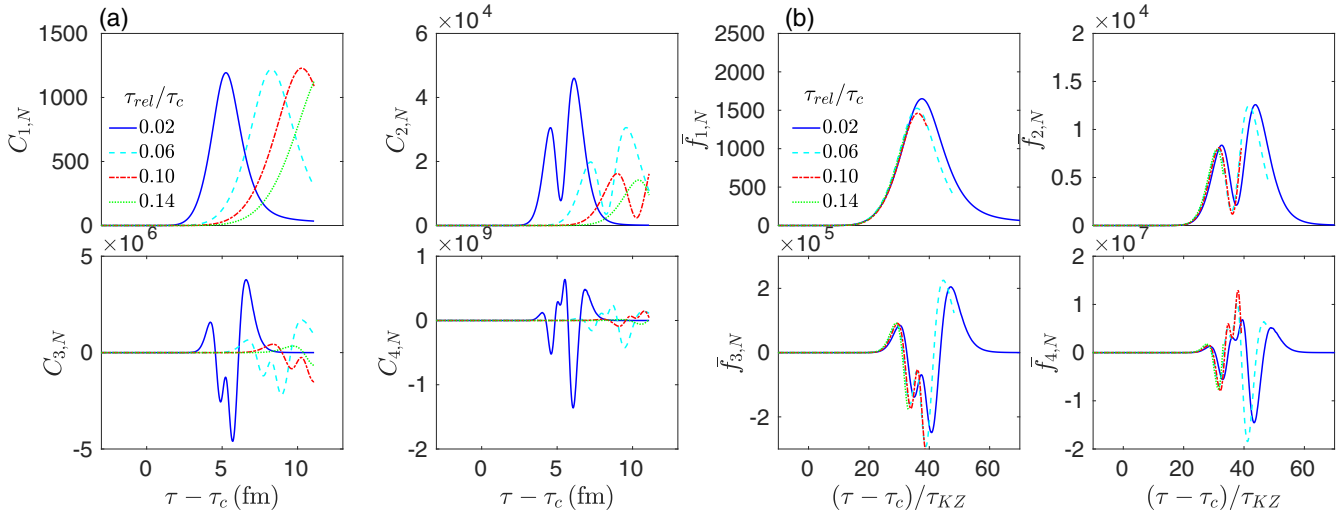

FIG. 5. (a) The cumulants $C_{n,N}$ $(n = 1, \ldots, 4)$ of net-protons as function of $\tau - \tau_c$, evolving along the trajectory of type A with $\tau_{\rm rel}/\tau_c = 0.02,\ 0.06,\ 0.10,\ 0.14$. (b) The corresponding universal functions $\bar{f}_{n,N}((\tau - \tau_{\rm c})/\tau_{\rm KZ}, \theta_{\rm KZ})$ $(n = 1, \ldots, 4)$ as a function of $(\tau - \tau_c)/\tau_{\rm KZ}$.

of type B with different r_c. Note that the formulas of the cumulants $C_{n,N}$, $(n = 1, \ldots, 4)$ for net-protons are similar to the ones of the σ field, but replace σ with $N_{p-\bar{p}}$ in Eq. (6). As the systems evolve near the critical point, higher order cumulants of net-protons show strong oscillations and the curves associated with different evolving trajectories largely separate from each other. In Figs. 5(b) and 6(b), we construct the corresponding possible universal functions $\bar{f}_{n,N}((\tau - \tau_{\rm c})/\tau_{\rm KZ}, \theta_{\rm KZ})$ $(n = 1, \ldots, 4)$ through rescaling the cumulants of net-protons and $\tau - \tau_c$ according to Eq. (9). Compared with the separating/oscillating $C_{n,N}$ curves in the left panels, the constructed $\bar{f}_{n,N}((\tau - \tau_{\rm c})/\tau_{\rm KZ}, \theta_{\rm KZ})$ approximately converge into one curve in Figs. 5(b) and 6(b).

IV. SUMMARY AND OUTLOOK

In this paper, we investigated the Kibble-Zurek scaling for the critical fluctuations of the σ field and net-protons within the framework of Langevin dynamics. We focused on two ideal cases: 1) the systems evolve along a chosen trajectory of type A with fixed chemical potential but with different relaxation times, 2) the systems evolve along different trajectories of type B that are associated with different r_c parameters. Our event-by-event simulations of the Langevin dynamics demonstrated that the cumulants C_n, $(n = 1, \ldots, 4)$ of the σ field are sensitive to both the relaxation times and evolving trajectories.

Using these traditional cumulants C_n, $(n = 1, \ldots, 4)$, we constructed the universal functions $\bar{f}_n((\tau - \tau_{\rm c})/\tau_{\rm KZ}, \theta_{\rm KZ})$ $(n = 1, \ldots, 4)$ of the σ field through rescaling the corresponding cumulants C_n and proper time $\tau - \tau_c$ with the the characteristic scales $\tau_{\rm KZ}$, $l_{\rm KZ}$, and $\theta_{\rm KZ}$ for the evolving systems. We found these constructed universal functions $\bar{f}_n$ are nicely overlapped each other in the critical regime for both case 1) and case 2), which are insensitive to the relaxation times and evolving trajectories, respectively.

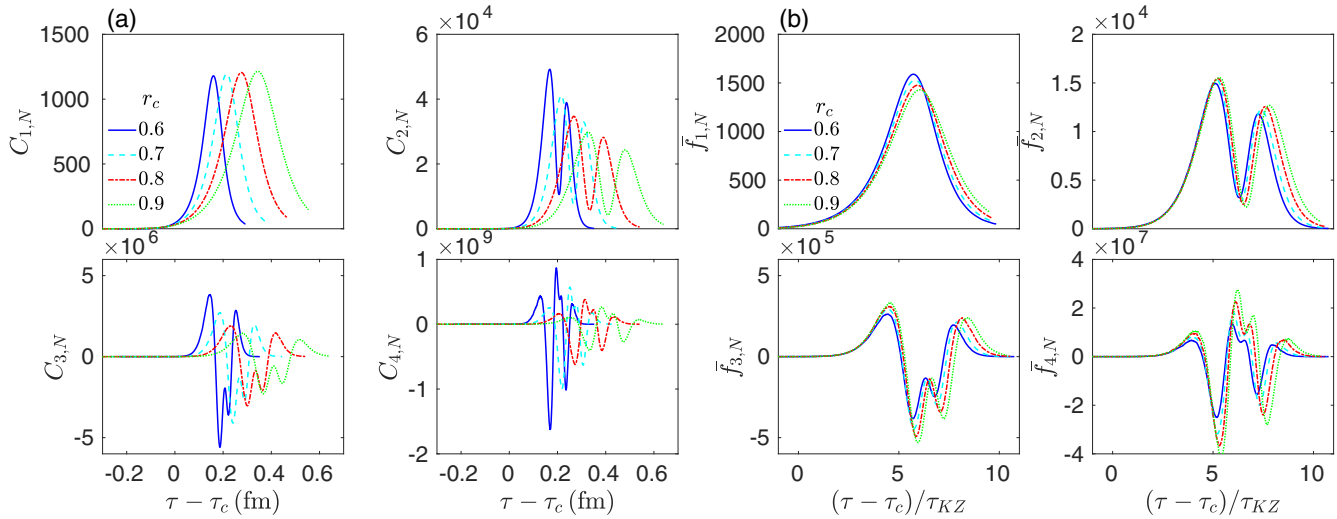

FIG. 6. Similar to Fig. 5, but evolving along type B trajectories with $r_c = 0.6,\ 0.7,\ 0.8,\ 0.9$.

For protons and antiprotons, the σNN coupling translate the critical fluctuations of the σ field to the critical fluctuations of net-protons. Correspondingly, the cumulants of net-protons are sensitive to both relaxation times and evolving trajectories as the case for the σ field. For small fluctuations of the σ field, we found the linear expansion of the classical distribution functions $f_{p/\bar{p}}$ directly transforms the universal scaling of the σ field to the universal scaling of net-protons. For large fluctuations of the σ field, the numerical calculations with the full distribution functions $f_{p/\bar{p}}$ have shown that the universal behavior of net-protons are slightly broken in the critical regime, but still drastically reduce the sensitivity to the relaxation time and evolving trajectories, which even change the oscillating behavior for higher cumulants of net-protons into an approximate universal curves.

Finally, we emphasis that this paper focuses on investigating the universal scaling of the σ field and net-protons for two ideal cases with specifically chosen trajectories, along which spatially uniform temperature T and chemical potential μ changes with the evolution time. These results cannot be directly compared with the experimental data that involve the complex QGP fireball evolution with inhomogeneous $T(\boldsymbol{x})$ and $\mu(\boldsymbol{x})$ changing in the whole positions space. Besides, we implement the Langevin dynamics of model A to simplify the numerical simulations, which only considers the evolution of nonconserved order parameter field near the critical point. The multiplicity fluctuations of net-protons are introduced through σNN coupling in the classical distributions functions (10), which cannot ensure the global charge conservation as the case in the traditional Cooper-Frye freeze-out scheme [52,53]. In the near future, such Kibble-Zurek scaling analysis should be extended to model B which directly evolves the conserved charges near the critical point. Besides, it is also worthwhile to develop sophisticated dynamical model near the critical point, such as hydro+, to further investigate the possible universal scaling of the experimental observables.

ACKNOWLEDGMENTS

We would like to thank the fruitful discussion with Y. Yin, S. Mukherjee, M. Stephanov, D. Teaney, and M. Asakawa. This work is supported by the NSFC and the MOST under Grant Nos. 11435001, 11675004, and 2015CB856900. S.W. is also partially supported by the Beam Energy Scan Theory (BEST) Topical Collaboration during his visit to BNL. We also gratefully acknowledge the extensive computing resources provided by the Super-computing Center of Chinese Academy of Science (SCCAS), Tianhe-1A from the National Supercomputing Center in Tianjin, China, and the High-performance Computing Platform of Peking University.

APPENDIX A: PARAMETERIZATION OF THE EFFECTIVE POTENTIAL FROM 3D ISING MODEL

The parameters $\sigma_0, m_\sigma, \lambda_3, \lambda_4$ in the effective potential Eq. (3) can be obtained from a mapping between the bot QCD systems and the 3d Ising model. In the 3d Ising model, the equilibrium cumulants $M^{\rm eq}(R,\theta), \kappa_n^{\rm eq}(R,\theta), n = 2, 3, 4, \ldots$ can be written as [46,47]

$$M^{\rm eq} = M_0 R^{1/3}\theta \equiv M_0 a_1, \tag{A1a}$$

$$\kappa_2^{\rm eq} = \frac{M_0}{V_4 H_0}\frac{1}{R^{4/3}(3+2\theta^2)} \equiv \frac{M_0}{V_4 H_0} a_2, \tag{A1b}$$

$$\kappa_3^{\rm eq} = \frac{-M_0}{(V_4 H_0)^2}\frac{4\theta(9+\theta^2)}{R^3(3-\theta^2)(3+2\theta^2)^3} \equiv \frac{-M_0}{(V_4 H_0)^2} a_3, \tag{A1c}$$

$$\kappa_4^{\rm eq} = \frac{-12 M_0}{(V_4 H_0)^3}\frac{81 - 783\theta^2 + 105\theta^4 - 5\theta^6 + 2\theta^8}{R^{14/3}(3-\theta^2)^3(3+2\theta^2)^5} \equiv \frac{-12 M_0}{(V_4 H_0)^3} a_4. \tag{A1d}$$

Here, R and θ are the distance and angle with respect to the location of the critical point and $V_4 \equiv V/T$ (for the detail derivation of Eqs. (A1), please refer to Appendix A of Ref. [29]). The cumulants of sigma field can also be calculated from the distribution function $P_0(\sigma) \sim \exp(-U_0(\sigma)/T)$, which take the forms

$$M^{\rm eq} = \sigma_0, \quad \kappa_2^{\rm eq} = \frac{\xi_{\rm eq}^2}{V_4}, \quad \kappa_3^{\rm eq} = -\frac{2\lambda_3}{V_4^2}\xi_{\rm eq}^6,$$
$$\kappa_4^{\rm eq} = \frac{6}{V_4^3}[2(\lambda_3\xi_{\rm eq})^2 - \lambda_4]\xi_{\rm eq}^8. \tag{A2}$$

Comparing Eqs. (A1) with Eqs. (A2) gives

$$\sigma_0(R,\theta) = M_0 a_1, \quad \xi_{\rm eq}^2(R,\theta) = 5\xi_{\rm min}^2 a_2,$$
$$\lambda_3(R,\theta) = \frac{1}{2}\frac{H_0}{M_0^2}\frac{a_3}{a_2^3}, \quad \lambda_4(R,\theta) = \frac{1}{2}\frac{H_0}{M_0^3}\frac{a_3^2}{a_2^5} + 2\frac{H_0}{M_0^3}\frac{a_4}{a_2^4}. \tag{A3}$$

In this work, M_0 and H_0 are two free parameters and we set $M_0 = 200$ MeV and $\xi_{\rm min} = 1$ fm.

With the linear parametric relation $r(R,\theta) = R(1-\theta^2)$, $h(R,\theta) = R^{5/3}(3\theta - 2\theta^3)$, the above $\sigma_0(R,\theta)$, $\xi_{\rm eq}^2(R,\theta)$, $\lambda_3(R,\theta)$, $\lambda_4(R,\theta)$ are converted into $\sigma_0(r,h)$, $\xi_{\rm eq}^2(r,h)$, $\lambda_3(r,h)$, $\lambda_4(r,h)$, which then can be mapped to the $T-\mu$ plane with the following linear transformation:

$$\frac{T-T_c}{\Delta T} = \frac{h}{\Delta h}, \quad \frac{\mu-\mu_c}{\Delta\mu} = -\frac{r}{\Delta r}, \tag{A4}$$

where the definitions and values of the parameters used in this paper are $\Delta T = T_c/8$, $\Delta\mu = 0.1$ GeV, $\Delta r = (5/3)^{3/4}$, $\Delta h = 1$, $T_c = 0.16$ GeV, and $\mu_c = 0.395$ GeV.

APPENDIX B: ANALYTICAL KIBBLE-ZUREK SCALING OF MODEL A

In this Appendix, we will analytically explain the Kibble-Zurek scaling of model A with a simplified Langevin equation, which is similar to Eq. (1), but neglect the higher order terms in the effective potential (3). Correspondingly, the evolution equation of the sigma field after the Fourier Transformation is written as

$$\frac{\partial\sigma(\boldsymbol{q},\tau)}{\partial\tau} = -\frac{1}{m_\sigma^2\tau_{\rm eff}}\left\{\boldsymbol{q}^2\sigma(\boldsymbol{q},\tau) + m_\sigma^2[\sigma(\boldsymbol{q},\tau) - \sigma_0]\right\} + \zeta(\boldsymbol{q},\tau), \tag{B1}$$

where the noise term in the Fourier space

$$\langle \zeta(\boldsymbol{q},\tau)\rangle = 0, \tag{B2}$$

$$\langle \zeta(\boldsymbol{q},\tau)\zeta(\boldsymbol{q}',\tau')\rangle = \frac{2(2\pi)^3 T}{m_\sigma^2 \tau_{\rm eff}}\delta^3(\boldsymbol{q}+\boldsymbol{q}')\delta(\tau-\tau'). \tag{B3}$$

With the inverse Fourier transform and the definition of Eq. (6), the evolution equation of the first and second order cumulant C_1, C_2 are written as[1]

$$\frac{\partial C_1}{\partial \tau} = -\frac{1}{\tau_{\rm eff}}[C_1 - \sigma_0], \tag{B4a}$$

$$\frac{\partial C_2}{\partial \tau} = -\frac{2}{\tau_{\rm eff}}\left[C_2 - \frac{\xi_{\rm eq}^2}{V_4}\right]. \tag{B4b}$$

Suppose the nonuniversal factor is incorporated in the characteristic scales $\tau_{\rm KZ}$, $l_{\rm KZ}$, and $\theta_{\rm KZ}$ and the associated variables is redefined as

$$\tilde{\tau} \equiv (\tau-\tau_c)/\tau_{\rm KZ}, \quad \tilde{\xi} \equiv \xi_{\rm eq}/l_{\rm KZ}, \quad \tilde{C}_1 \equiv C_1/l_{\rm KZ}^{-1/2},$$
$$\tilde{C}_2 \equiv C_2/l_{\rm KZ}^2. \tag{B5}$$

The above dynamical equation (B4) can be rewritten as

$$\frac{\partial \tilde{C}_1}{\partial \tilde{\tau}} = -\frac{\tau_{\rm KZ}}{\tau_{\rm rel} l_{\rm KZ}^z (\tilde{\xi}/\xi_{\rm min})^z}[\tilde{C}_1 - \tilde{\sigma}_0], \tag{B6a}$$

$$\frac{\partial \tilde{C}_2}{\partial \tilde{\tau}} = -2\frac{\tau_{\rm KZ}}{\tau_{\rm rel} l_{\rm KZ}^z (\tilde{\xi}/\xi_{\rm min})^z}\left[\tilde{C}_2 - \frac{\tilde{\xi}_{\rm eq}^2}{V_4}\right], \tag{B6b}$$

Here, V_4 is assumed to be a constant and we use the form $\tau_{\rm eff} = \tau_{\rm rel}(\xi_{\rm eq}/\xi_{\rm min})^z$ for the effective relaxation time $\tau_{\rm eff}$. The above Eqs. (B6) show that if one could eliminate the nonuniversal factor $\tau_{\rm KZ}/(\tau_{\rm rel} l_{\rm KZ}^z)$, $\tilde{C}_1$ and $\tilde{C}_2$ as a function of $\tilde{\tau}$ become universal, respectively. In the following part of this section, we will show that the typical definition of $\tau_{\rm KZ}$ within the framework of KZM will ensure the universality of $\tilde{C}_1$ and $\tilde{C}_2$ for both Type A and Type B trajectories.

For the trajectory of Type A with $r \simeq 0$, $\theta \simeq \pm 1$, one finds that $\xi_{\rm eq} \sim t^{-2/5}$ from Eqs. (A1), (A4), and (5). Therefore,

$$\tau_{\rm quench}^{\xi} = \left|\frac{\xi_{\rm eq}}{\partial_\tau \xi_{\rm eq}}\right| \sim \frac{5}{2}t, \tag{B7}$$

where $t \equiv \tau - \tau_c$. As defined in Eqs. (8) for these characteristic scales

$$\tau_{\rm KZ} = \tau_{\rm quench}^{\xi} = \tau_{\rm eff} = \tau_{\rm rel}\left(\frac{\xi_{\rm eq}}{\xi_{\rm min}}\right)^z. \tag{B8}$$

Then, one could obtain

$$\tau_{\rm KZ} = \tau_{\rm rel} l_{\rm KZ}^z, \tag{B9}$$

which just eliminate the nonuniversal factor in Eq. (B6) near the critical point.

For the trajectory of Type B, the equilibrium correlation length varies slowly, and $\tau_{\rm quench}^{\xi}$ is large. With $\theta \sim \tau - \tau_c = t$, the quench time is

$$\tau_{\rm quench}^{\theta} = \left|\frac{\theta}{\partial_\tau \theta}\right| \sim t, \tag{B10}$$

and with the same condition (B8), we obtained the the same relation described by Eq. (B9), which eliminate the nonuniversal factor in Eq. (B6).

[1]The cumulants of C_3 and C_4 are zero for the simplified Langevin equation (B1) without higher order terms.

[1] M. A. Stephanov, K. Rajagopal, and E. V. Shuryak, Phys. Rev. Lett. **81**, 4816 (1998).
[2] M. M. Aggarwal *et al.* (STAR Collaboration), arXiv:1007.2613.
[3] M. A. Stephanov, Prog. Theor. Phys. Suppl. **153**, 139 (2004).
[4] M. A. Stephanov, PoS LAT **2006**, 024 (2006).
[5] M. Asakawa and M. Kitazawa, Prog. Part. Nucl. Phys. **90**, 299 (2016).
[6] X. Luo and N. Xu, Nucl. Sci. Tech. **28**, 112 (2017).
[7] S. P. Klevansky, Rev. Mod. Phys. **64**, 649 (1992).
[8] K. Fukushima, Phys. Lett. B **591**, 277 (2004).
[9] W. J. Fu, Z. Zhang, and Y. X. Liu, Phys. Rev. D **77**, 014006 (2008).
[10] L. J. Jiang, X. Y. Xin, K. L. Wang, S. X. Qin, and Y. X. Liu, Phys. Rev. D **88**, 016008 (2013).
[11] C. D. Roberts and A. G. Williams, Prog. Part. Nucl. Phys. **33**, 477 (1994).
[12] S. X. Qin, L. Chang, H. Chen, Y. X. Liu, and C. D. Roberts, Phys. Rev. Lett. **106**, 172301 (2011).
[13] J. Berges, N. Tetradis, and C. Wetterich, Phys. Rep. **363**, 223 (2002).
[14] M. A. Stephanov, K. Rajagopal, and E. V. Shuryak, Phys. Rev. D **60**, 114028 (1999).
[15] M. A. Stephanov, Phys. Rev. Lett. **102**, 032301 (2009).
[16] M. A. Stephanov, Phys. Rev. Lett. **107**, 052301 (2011).
[17] M. M. Aggarwal *et al.* (STAR Collaboration), Phys. Rev. Lett. **105**, 022302 (2010).
[18] L. Adamczyk *et al.* (STAR Collaboration), Phys. Rev. Lett. **112**, 032302 (2014).
[19] L. Adamczyk *et al.* (STAR Collaboration), Phys. Rev. Lett. **113**, 092301 (2014).
[20] J. Thäder (STAR Collaboration), Nucl. Phys. A **956**, 320 (2016).
[21] X. Luo (STAR Collaboration), PoS CPOD **2014**, 019 (2015).
[22] B. Berdnikov and K. Rajagopal, Phys. Rev. D **61**, 105017 (2000).
[23] K. Paech, H. Stocker, and A. Dumitru, Phys. Rev. C **68**, 044907 (2003).

[24] D. T. Son and M. A. Stephanov, Phys. Rev. D **70**, 056001 (2004).
[25] C. Nonaka and M. Asakawa, Phys. Rev. C **71**, 044904 (2005).
[26] M. Asakawa, S. Ejiri, and M. Kitazawa, Phys. Rev. Lett. **103**, 262301 (2009).
[27] M. A. Stephanov, Phys. Rev. D **81**, 054012 (2010).
[28] M. Nahrgang, S. Leupold, C. Herold, and M. Bleicher, Phys. Rev. C **84**, 024912 (2011).
[29] S. Mukherjee, R. Venugopalan, and Y. Yin, Phys. Rev. C **92**, 034912 (2015).
[30] L. Jiang, S. Wu, and H. Song, Nucl. Phys. A **967**, 441 (2017).
[31] B. Ling and M. A. Stephanov, Phys. Rev. C **93**, 034915 (2016).
[32] L. Jiang, P. Li, and H. Song, Phys. Rev. C **94**, 024918 (2016).
[33] S. Mukherjee, R. Venugopalan, and Y. Yin, Phys. Rev. Lett. **117**, 222301 (2016).
[34] M. Sakaida, M. Asakawa, H. Fujii, and M. Kitazawa, Phys. Rev. C **95**, 064905 (2017).
[35] J. Brewer, S. Mukherjee, K. Rajagopal, and Y. Yin, Phys. Rev. C **98**, 061901(R) (2018).
[36] M. Stephanov and Y. Yin, Phys. Rev. D **98**, 036006 (2018).
[37] Y. Akamatsu, D. Teaney, F. Yan, and Y. Yin, arXiv:1811.05081.
[38] M. Nahrgang, M. Bluhm, T. Schaefer, and S. A. Bass, arXiv:1804.05728.
[39] A. Chandran, A. Erez, S. S. Gubser, and S. L. Sondhi, Phys. Rev. B **86**, 064304 (2012).
[40] M. Kolodrubetz, B. K. Clark, and D. A. Huse, Phys. Rev. Lett. **109**, 015701 (2012).
[41] A. Francuz, J. Dziarmaga, B. Gardas, and W. H. Zurek, Phys. Rev. B **93**, 075134 (2016).
[42] G. Nikoghosyan, R. Nigmatullin, and M. B. Plenio, Phys. Rev. Lett. **116**, 080601 (2016).
[43] T. W. B. Kibble, J. Phys. A: Math. Gen. **9**, 1387 (1976).
[44] W. H. Zurek, Nature **317**, 505 (1985).
[45] P. C. Hohenberg and B. I. Halperin, Rev. Mod. Phys. **49**, 435 (1977).
[46] J. Zinn-Justin, Phys. Rep. **344**, 159 (2001).
[47] P. Schofield, J. D. Litster, and J. T. Ho, Phys. Rev. Lett. **23**, 1098 (1969).
[48] N. C. Cassol-Seewald, R. L. S. Farias, E. S. Fraga, G. Krein, and R. O. Ramos, Physica. A **391**, 4088 (2012).
[49] C. Herold, M. Nahrgang, Y. Yan, and C. Kobdaj, Phys. Rev. C **93**, 021902(R) (2016).
[50] S. Wu and H. Song (unpublished).
[51] Z. Fodor and S. D. Katz, J. High Energy Phys. 04 (2004) 050.
[52] J. Li, H. J. Xu, and H. Song, Phys. Rev. C **97**, 014902 (2018).
[53] C. Schwarz, D. Oliinychenko, L.-G. Pang, S. Ryu, and H. Petersen, J. Phys. G **45**, 015001 (2018).